Proteomic Analysis Defines Kinase Taxonomies Specific for Subtypes of Breast Cancer

K. A.L. Collins[1†], T. J. Stuhlmiller[2,3†], J. S. Zawistowski[2], M. P. East[2], T. Pham[2,3], C. R. Hall[4], D. R. Goulet[2], S. M. Bevill[2], S. P. Angus[2], S. H. Velarde[2,3], N. Sciaky[2], L. M. Graves[2], G. L. Johnson[2,3]*, S. M. Gomez[1,2,4]*

[1]Curriculum in Bioinformatics and Computational Biology, University of North Carolina at Chapel Hill, Chapel Hill, NC 27514.

[2]Department of Pharmacology, University of North Carolina at Chapel Hill, Chapel Hill, NC 27514.

[3]Lineberger Comprehensive Cancer Center, University of North Carolina at Chapel Hill, Chapel Hill, NC 27514.

[4]Joint Department of Biomedical Engineering, University of North Carolina at Chapel Hill and North Carolina State University, Chapel Hill, NC 27514.

*To whom correspondence should be addressed: gary_johnson@med.unc.edu and smgomez@unc.edu

†These authors contributed equally to this work.

Abstract

Multiplexed small molecule inhibitors covalently bound to Sepharose beads (MIBs) were used to capture functional kinases in luminal, HER2-enriched and triple negative, basal-like and claudin-low breast cancer cell lines and tumors. Kinase MIB-binding profiles at baseline without perturbation were significantly uncorrelated to transcript abundance for many kinases and proteomically distinguished the four breast cancer subtypes. Understudied kinases were highly represented in the MIB-binding taxonomies and shown to be integrated in kinase signaling subnetworks with characterized kinases. Computationally it was possible to define subtypes using profiles of only 50 of the more than 300 kinases bound to MIBs that included understudied as well as metabolic and lipid kinases (22 of 50 were understudied). MIB-binding profiles readily defined subtype-selective differential adaptive kinome reprogramming in response to targeted kinase inhibition. Comprehensive MIBs-based capture of kinases provides a unique proteomics-based method for defining functional kinome dynamics and subnetworks in cells and tumors that integrates poorly characterized kinases of the understudied kinome that is not possible using genomic strategies.

Introduction

Breast cancer has two primary subtypes that includes luminal A and B as well as the majority of HER2+ breast cancers and triple negative breast cancer (TNBC) that can be divided into basal-like and claudin-low [1]. Interestingly, basal-like breast cancer using molecular taxonomies is as different from luminal and HER2+ breast cancers as lung cancer, leading to the proposal that basal-like breast cancers are in fact a unique disease [2], [3]. Estrogen and progesterone receptor dependence and HER2 addiction define vulnerabilities in luminal/HER2+ breast cancers. However, in basal-like and claudin-low triple negative breast cancer, there are no oncogenic drivers that define a vulnerability that can be therapeutically targeted.

Even with the growing databases of genomic information for breast cancers, it is often still unclear how molecular taxonomies translate to phenotype. Additional methods characterizing proteomic taxonomies are needed to understand signaling networks, particularly of protein kinases due to their druggability. Important for this analysis of the breast cancer kinome is a characterization of understudied kinases, representing nearly half of the kinome and lacking essential functional characterization as well as molecular tools for their manipulation and study [4]. These understudied kinases need to be functionally integrated into kinase networks for a global understanding of kinome dynamics to be achieved both at baseline and in response to perturbation.

To this end, we have developed methods using multiplexed inhibitor beads (MIBs) coupled with mass spectrometry (MIB/MS) that have the ability to bind and identify a large percentage of kinases in the human kinome [5], [6]. By RNA-seq, most cell lines express 350 or so kinases and our MIB-binding profiling captures a significant percentage of the expressed kinome [7]. In the current study we have compiled the baseline kinase MIB-binding profile using MIB/MS for 15 cell lines across breast cancer subtypes in addition to patient tumors. Using feature selection methodologies, it was possible to define kinase taxonomies for breast cancers based on the MIB/MS profile of 50 kinases among the kinases captured by MIB/MS that includes understudied protein kinases, lipid and metabolic kinases. Using the baseline MIB-binding state in a machine-learning framework further allows accurate classification of breast cancer in both cell lines and primary tumors. Kinases identified within these distinguishing profiles are distributed throughout the kinome, representing multiple subnetworks with a significant representation of understudied kinases. The findings demonstrate that determining the functional kinome based on MIB-binding has prognostic value in defining the integration of signaling networks that is not currently possible using genomic strategies.

Results

Multiplexed Kinase Inhibitor Beads capture kinases from every subfamily and provide a means to assay understudied kinases

Multiplexed kinase inhibitor beads (MIBs) are a set of Sepharose beads each with a specific covalently-attached kinase inhibitor [8], [9]. Coupling MIB gravity-flow affinity chromatography with mass spectrometry (MIB/MS) provides the ability to capture and identify kinases from whole cell lysates on a kinome scale. Binding of kinases is dependent on the functional

expression of the kinase and affinity for the different immobilized inhibitors. To determine the inhibitor bead selective distribution of bound kinases, we assayed kinase capture by six different inhibitors individually covalently coupled to Sepharose beads [6], [8]: CTx-0294885, VI-16832, PP58, Purvalanol B, and two custom synthesized molecules, UNC-8088A and UNC-2147A. Four cell lines representative of breast cancer subtypes: HCC1806 (basal-like), SUM159 (claudin-low), MCF7 (luminal), and SKBR-3 (HER2-enriched) were used for analysis (Figure 1A). Of these, CTx-0294885 (CTx) and VI-16832 (VI) captured the most total kinases (265 and 254, respectively) and the most unique kinases (32 and 29, respectively). The other four beads bound a lesser number of kinases (PP58, 194 kinases; Purvalanol B, 164; UNC-8088A, 162; UNC-2147A, 130, Figure 1B, Table S1). Although UNC-8088A binds the fewest unique kinases (only five), these include the atypical bromodomain and extraterminal (BET) domain-containing family of chromatin readers BRD2, -3, and -4 [10]. Hierarchical clustering of identified kinase peptides shows each bead binds a unique set of kinases and UNC-2147A displays the most distinct binding profile selectively enriching the AGC kinases (Figure 1C).

Understudied kinases make up a large proportion of kinases captured across the inhibitor beads, ranging from 23-34% of all kinases captured for any individual bead (Figure 1D). Understudied kinases [4] represent approximately 40% (Table S2) of the expressed kinome. Characteristics of understudied kinases includes: i) integration of the protein kinase in signaling networks is poorly defined, ii) function and/or regulation is poorly defined, iii) activation loop phospho-antibodies and/or IHC grade antibodies may not exist, iv) lack of selective chemical tools for use in characterization of function (e.g., small molecule inhibitors), v) RNAi and CRISPR/Cas9 for knockout/altered expression and cDNAs for overexpression may be primary tools, vi) kinase knockout or altered expression may not provide readily assayable phenotypes (e.g., growth, migration, apoptosis or in vivo function in mouse organ physiology).

Across all MIB/MS runs, 381 kinases in total were identified. Of these, 35 are metabolic and lipid kinases, 346 are protein kinases of which 142 can be considered understudied (41% of protein kinases identified) (Figure 1E). The overall distribution of kinases bound indicates CTx and VI are clearly pan-kinase inhibitors (Figure 1F, circle size proportional to number of unique peptides identified per kinase). Purvalanol B also binds kinases across families but to a lesser extent. PP58 has some preference for tyrosine kinases (TKs), and UNC-8088A has preference for TKs, CMGC, and atypical kinases over other families. UNC-2147A, designed for interaction with the binding pocket of AKT, has a strong affinity for AGC kinases lacking in most of the other five kinase inhibitors. CTx, VI, and PP58 have a strong affinity for the PRKDC (DNA-PK) not seen with the other three inhibitors. All inhibitor beads display high affinity for many understudied kinases (green circles and text). The most-highly captured understudied kinases across the four cell lines were GAK, SLK, MRCKB, AAK1, TBK1, and NEK9.

Kinases known to be oncogenic drivers in general and/or nodal signaling kinases display anticipated MIB-binding profiles across the different breast cancer subtype cell lines (Figure 1G). For example, SKBR3 (luminal HER2+) and MCF7 (luminal) cells have abundant AKT1/2 MIB-binding. Other well-characterized kinases are highly represented in a specific cell line, such as EGFR and FAK1 in HCC1806, EPHA2 and UFO (AXL) in SUM159, IGF1R and KS6B1 (p70 S6K) in MCF7, and HER2/ERBB2 and TGFBR1 in SKBR-3 cells. Several understudied kinases also show high selectivity in functional MIB-binding including CDK13, DMPK, SIK3

and TESK1 in MCF7 and CLK4, CDK14 and NLK in SUM159 cells (Figure 1H). Figure 1I and Table S1 show kinases whose MIB-binding is greatest in each of the four cell lines, proportional to the number of unique peptides identified. Unsupervised hierarchical clustering illustrates the differences in MIB-binding throughout the kinome for each cell line (Figure 1J). These findings indicate the four cell lines display a unique MIB/MS binding profile for both well-characterized and understudied kinases.

Integrating understudied and well-characterized kinases by kinome proteomic profiling defines breast cancer subtypes

We characterized the baseline kinome of 15 breast cancer cell lines representing the four major breast cancer subtypes defined by gene expression profiles [1]. Cell lysates were passed over an affinity column composed of the six kinase inhibitor beads and processed for LC-MS/MS (Figure 2A). Using label-free peptide quantitation measurements a total of 360 kinases were identified having at least 3 unique peptides (Data file S1). Claudin-low and basal-like cells (TNBC) are readily distinguished from HER2-enriched/luminal cells by MIB profiling of the cellular kinomes shown by consensus clustering in Figure 2B. The basal-like HER2-amplified cell line HCC1954 clusters with basal-like lines by kinome profile and is thus separated from the luminal HER2+ lines. Interestingly, the SKBR-3 HER2-enriched cell line shows an intermediate clustering between HCC1954 and other HER2+/luminal cell lines, and a previous report demonstrated SKBR-3 patterns as basal-like in functional RNAi screens [11]. Hierarchical clustering of kinases further separated cell lines with the claudin-low phenotype, SUM159, MDA-MB-231 and MDA-MB-468 (basal-like), showing the greatest difference from other cell lines (Figure 2C). SUM229 cells have two subpopulations, a basal-like EpCAM positive/E-cadherin positive (SUM229pos) and a claudin-low EpCAM negative/E-cadherin negative population (SUM229neg). The two populations are genomically similar by exome sequencing, but differ epigenetically [12] and cluster together based on their kinome MIB-binding profile (Figure 2C).

Principal components analysis (PCA) of baseline MIB-binding kinase profiles revealed significant differences between subtypes within the first principal component, clearly separating triple-negative from HER2-enriched and luminal cell lines (Figure 2D). Further separation of the triple-negative group into claudin-low and basal subtypes is also readily achieved. Appreciable separation of HER2-enriched cell lines from luminal cell lines is observed in the second principal component, as is that of the basal-like/HER2-amplified cell lines from the basal-like and claudin-low lines. A loadings plot, which defines relationships between MIB-binding for each kinase, highlights those kinases with significant variation within subtypes, with numerous understudied kinases being apparent (Figure 2E). Examples of understudied kinases with differences in MIB-binding among cell lines include ADCK1, PKN3, STK17A and TESK1. Similarly, well-characterized kinases known for their relevance in breast cancer are observed, such as ERBB2, EPHA1, MET and TGFBR2.

Supervised differential expression analysis of MIB-captured kinases from claudin-low/basal-like (TNBC) versus HER2/luminal cell lines defined several statistically significant differences (Figure 2F). Multiple Ephrin receptors (EPHA2/A7/B2) and members of the TGF-beta superfamily (TGFBR2, ACVR1) are among the kinases most associated with TNBC while ERBB3 and RET are over-represented in HER2+ and luminal cell lines. Many understudied

kinases display higher MIB-binding in HER2+/luminal cells, including DMPK, ADCK1, and TESK1. Individual plots for selected kinases are shown in Figure 2G, showing distinctive patterns of MIB-binding across subtypes.

Kinase MIB-binding activity is independent from mRNA expression level

Our results clearly demonstrate that kinase MIB-binding displays strong variation across breast cancer subtypes. Global gene expression measurements have similarly shown subtype-specific dynamics, with expression of selected gene sets being utilized in subtype determination and diagnosis [13]–[15]. We compared baseline RNA-seq measurements with corresponding MIB-capture of protein kinases to assess the relationship between transcript abundance and functional kinome behavior. Comparison of kinase transcript expression with MIB-binding using label-free quantitation of kinase peptide abundance for each subtype showed relatively low correspondence, with correlation coefficients of 0.25 or below, implying that less than 7% of the observed variation between MIB-binding and RNA abundance in breast cancer subtypes is explained through this relationship (Figure 3A-D). These results are consistent with earlier work that found the average correlation between gene expression and protein abundance in TCGA colorectal cancer samples to be approximately 0.47, with a lesser correlation of 0.23 when comparing gene expression and protein variation [16]. The low correlation between RNA-seq and MIB-binding suggests that the use of MIB/MS provides a picture of kinome behavior complementary to that provided through expression measures. In particular, these results support the potentially significant role of post-translational and transcriptional regulation in kinome dynamics [17] [18]. The relationship between these two measures is shown as a scatter plot for cell lines representing the basal subtype in Figure 3A (left panel), with the Z-scores for both read count and MIB-binding plotted on the x- and y-axes, respectively, and further emphasize the lack of strong correlation between these two measures of kinase behavior. Kinases along the gray line (y=x) represent those where transcript expression directly corresponds to MIB-binding (i.e. a unit increase in expression corresponds to a unit increase in MIB-binding). A point above the gray line in the scatter plot indicates a kinase that has more MIB-binding than expected given the expression level of that kinase in that subtype; these kinases are referred to as “functionally dominant” for their increased MIB-binding relative to transcript expression. Examples of functionally dominant kinases in the basal-like subtype are KCC2A, HCK, and EPHA5; in the claudin-low subtype KCC2A, MK10, and FGFR2; in the HER2-enriched subtype KCC2A, HCK, and EPHB1; and in the luminal subtype KCC2A, HCK, and FYN. Similarly, points below the gray line indicate kinases that have less MIB-binding than expected given the expression level of that kinase and are labeled as “expression dominant” kinases. Examples of expression dominant kinases include KPYM, TIF1B and K6PL. The significant number of both functionally and expression dominant kinases common across several subtypes is readily detected by MIB/MS and suggests a post-transcriptional regulation of different kinases likely related to differential covalent regulatory modifications and protein stability. Such proteomic behavioral properties can not be detected by RNA-seq. In addition, recombinant kinases often used to profile on-target/off-target inhibitor profiles are not representative of endogenous kinases in cell lysates that have associated regulatory subunits and post-translational modifications [19], [20]. These data describing endogenous kinases captured in cell lysates by MIBs provides an integrated perspective, with both understudied and well-characterized kinases having similar functional versus expression dominant properties as well as demonstrating the potential for common mechanisms of regulation. Furthermore, the properties of a subset of characterized and

understudied kinases suggest the dynamic regulation of a subset of the kinome not previously detected using other methods.

In contrast to the lack of correlation between expression and MIB-binding of specific kinases, there are a significant subset of kinases that show a high MIB-mRNA correlation across cell lines, including some having a correlation value greater than 0.8. These include ERBB2, expressed at high levels in HER2+ breast cancer, as well as PDPK1and several other kinases such as PKN1 and others (Figure 3E), consistent with these kinases having transcriptional regulation as an important component of their overall functional output. Similar to the low correlation observed in Figure 3A-D, the distribution of the Pearson correlation coefficients of all kinases across all 15 cell lines shows a low correspondence between MIB-binding and RNA-seq (Figure 3F), with the mean correlation being 0.2. As also observed in Figure 3G there are a number of kinases that are only observed with one of the applied methods, MIB/MS or RNA-seq. This discrepancy is partly due to the 50+ RSEM read threshold used here as a positive identification in RNA-seq, potentially missing very lowly expressed kinases. Similarly, kinases not observed with MIB/MS but identified in RNA-seq may be missed due to being in an inactive, nonfunctional state and/or failure of chosen inhibitors to bind these kinases with adequate affinity. Pseudokinases that do not bind ATP will generally not be captured by MIBs.

Kinome profiles accurately define tumor biopsies

Cumulatively, our data show measurement of kinases by MIB capture allows integration of a significant fraction of the expressed kinome, including both understudied and well-characterized kinases. MIB-binding profiles define a taxonomy of breast cancer determined by the functional behavior of protein kinases. This functional taxonomy is used below to define subnetworks within the kinome that integrates understudied and well-characterized kinases that is not possible using transcriptome data.

Given both the variation in kinase MIB-binding profiles observed across subtypes, as well as their differing information content when compared to RNA expression measurements, we sought to better understand which kinases were key nodes in the subtype-selective baseline breast cancer kinome. To address this question we investigated the MIB-binding behavior of kinases across all four subtypes. We predicted three major classes of kinases: 1) those that show variation in MIB-binding across all subtypes, 2) those that exhibit more limited subtype-specific behaviors, and 3) kinases that have nominal distinguishing behavior. Standard application of PCA identifies those kinases displaying the greatest variation across all samples ("pan-subtype kinases"; Figure 2E) and thus we used a feature selection approach based on the Bhattacharyya distance [21] to determine subtype-specific kinases that are highly distinguishing/informative for a single cancer subtype (see Methods). The combined set of the 50 most informative kinases is shown in Figure 4A, with column ordering based on similarity of the kinome profile and recapitulating similarity between claudin-low and basal subtypes as well as HER2-enriched and luminal. The HER2+ cell line that profiles as basal-like (HCC1954, in purple) is displayed separately. Recognized cancer-related kinases are again observed in this set, including ERBB2, FGFR2, PTK6, RAF1 and RON (MST1R) as well as 22 understudied kinases. Using the 50 most informative pan- and subtype-specific kinases in Figure 4A, we assessed their effectiveness in subtype identification using a support vector machine (SVM) classifier along with leave-one-out cross-validation. We found that the ability to classify a cell line's subtype from measurement of

these kinases was highly accurate, with perfect precision and specificity for claudin-low and basal subtypes (Table S3).

The kinases shown in Figure 4A have the greatest variation within and across subtypes and are representative of each of the major subfamilies of kinases in addition to three metabolic kinases captured by MIBs (Figure 4B). Under the assumption that TNBC (represented by basal/claudin-low cell lines) and HER2/luminal breast cancer are separate diseases, we again used unsupervised feature selection of MIB/MS data to identify kinases that distinguish TNBC (basal/claudin-low) from HER2/luminal breast cancer [21]. As shown in Figure 4C, obvious differences in the kinome profiles of TNBC and HER2/luminal are observed, demonstrating the unique functional phenotypic features of the kinome in the two different breast cancers. Sixteen understudied kinases showed strong variance between TNBC and HER2/luminal breast cancer, with higher-ranked understudied kinases being DAPK3, ADCK1, MRCKA (CDC42BPA), STK17A, DMPK and VRK2.

Using the kinases chosen from feature selection in Figure 4C, we evaluated the ability to use MIB-binding profiles to define subtypes of human HER2+ needle biopsies and TNBC breast tumors (Figure 4D & E). Diagnostic needle biopsies of 2 patient tumors (2 HER2+) having ~1 mg of total protein were processed using MIB enrichment. With just 1 mg of tumor lysate protein, the total number of kinases purified from each biopsy ranged from ~200 to 275. Utilizing the kinases in Figure 4C in a SVM classifier, it was possible to clearly identify HER2+ and TNBC primary patient tumors. As with cell lines, application of PCA to MIB-binding profiles showed a clear separation between TNBC tumors and HER2+ tumors (Figure 4F). Kinases driving the variation within the data included ERBB2 as expected and several understudied kinases including TESK1 and DMPK (Figure 4G). Thus, the MIB-binding activity of as few as 50 kinases is sufficient to discriminate the functional phenotypic nature of the kinome in breast cancer.

A functional interaction network of MIB-binding kinases

To determine the basic architecture of the kinome using MIB-bound kinases, we compiled protein interaction and phosphorylation data from multiple data sources (HIPPIE, HPRD, I2D, PhosphoSitePlus, Reactome; see Methods) and established a functional interaction network among 246 of the 254 kinases commonly identified in the panel of 15 breast cancer cell lines. Spectral clustering of this network further enabled the identification of 16 subnetworks (Figure 5A). Understudied kinases (green glyphs) are widely distributed across all the major subnetworks, demonstrating these poorly characterized kinases are integrated into subnetworks with well-characterized kinases. The 50 distinguishing kinases identified for cell lines in Figure 4A (triangle glyphs) were also distributed throughout the network and associated subnetworks. The scope of subnetwork coverage by these kinases suggests that their predictive value in our subtype classification comes from their distribution across many subnetworks, providing an overall estimate of the state of many functional processes simultaneously. Example subnetworks with enriched GO terms for the innate immune response (subnetwork 1) and cell division and mitosis (subnetwork 2) are shown in Figures 5B and 5C, respectively.

Kinome MIB-binding profile and response to drug perturbation
To assess how the baseline kinome and associated understudied kinases change in their functional MIB-binding profile in response to targeted drug perturbation, we exposed four cell lines to three subtype-relevant kinase inhibitors: SUM159 and HCC1806 with trametinib (a MEK1/2 inhibitor); SKBR3 with lapatinib (a HER2/EGFR inhibitor); and MCF7 with buparlisib (a PI3K inhibitor). The four inhibitors each strongly inhibited growth of the treated cell line (Figure 6A). We have previously shown that the kinome is dynamic and rapidly adapts to targeted perturbation by kinase inhibitors [5], [6]. This adaptive response is readily observed by changes in the MIB-binding profiles for each drug treatment (Figure 6B, Data file S3), with SUM159 cells showing the strongest dynamic response to drug perturbation relative to the other cell lines, but each line clearly shows an adaptive response of the kinome measured by MIB-binding profiles. Figure 6C shows the kinases that are unique to each subtype defined in Figure 2C (Table S4).

Scatter plots of the SUM159 and HCC1806 dataset defines specific kinases and kinome subnetworks that drive the adaptive response to MEK1/2 inhibition that are represented by both understudied and well-characterized kinases (Figure 6D). Understudied (i.e. NEK2 and PASK) and well-characterized (i.e. DDR1 and EPHA4) kinases respond differently in the two subtypes (basal-like and claudin-low) when they are treated with the same kinase inhibitor (trametinib). The kinases in the subnetworks defined in Figure 5 also respond uniquely in the basal-like and claudin-low subtypes when treated with trametinib (Figure 6E). The adaptive kinome response measured by dynamic changes in MIB-binding profiles is more clearly seen when specific subnetworks are analyzed (Figure 6F). The global response of the seven largest subnetworks to these drug perturbations is shown with their functional annotation as estimated from Gene Ontology terms and KEGG pathway enrichment shown on the x-axis and MIB-binding response reported on the y-axis as a mean across all cell lines and drugs. Subnetworks have heterogeneous responses, with some subnetworks being fairly coordinated in response and others having kinase members acting in a more strongly divergent manner. For instance, subnetwork 3 (SN3) is enriched with many kinases relevant to cytoskeleton, adhesion and motility and has many of its members strongly up-regulated in response to drug perturbation. In comparison, SN2, involved in cell cycle and cell division, contains both strongly up-regulated and down-regulated kinases, with the largest responses being loss of MIB-binding, consistent with the inhibition of cell growth. Understudied kinases (green labels in Figure 6F) often display large responses to drug treatment within a given subnetwork, demonstrating these kinases actively contribute to adaptive kinome reprogramming in response to targeted kinase inhibition. Similarly, a more detailed look at targeted inhibition of specific subnetworks for each of the cell lines shows the dynamic response of the kinome to be highly dependent on the drug, subtype and subnetwork context (Figure 6G, Table S5). More broadly, the response of kinases in subnetworks is consistent with a unique functional regulation of the kinome in cancer subtypes and in response to different perturbations.

Discussion

While the creation of molecular taxonomies has established the existence of subtypes in many tissue-specific cancers, how these taxonomies can be leveraged to characterize phenotype or to

guide the development of targeted therapeutics remains unclear. A complication for improving therapeutic intervention with targeted kinase inhibitors in cancer is the extensive number of understudied kinases, whose poor characterization presents significant challenges to understanding their role in emergent processes such as adaptive bypass reprogramming and resistance to kinase inhibitors. Despite such challenges, understudied kinases do have the potential as novel drug targets once their functional integration into signaling networks is more clearly determined. Methods generally have been lacking to capture kinases, both well-characterized and understudied, to define the functional kinome en masse. Characterization of kinase MIB-binding in tumor cell lysates has proven to be a powerful technique for characterizing functional architectures of the kinome that provides the capability to identify prognostic signatures and differential response to perturbations such as targeted kinase inhibition, as well as better establishing the integration and function of understudied kinases. This is clearly seen in the 50 kinase profile distinguishing TNBC from HER2+/luminal breast cancer with many of the 50 kinases representing understudied kinases.

The highest weighted understudied kinases distinguishing TNBC from HER2+/luminal breast cancer include ADCK1 (AarF Domain Containing Kinase whose function is unclear), DAPK3 (Death-associated protein kinase thought to be involved in apoptosis), DMPK (Dystrophia myotonica protein kinase whose function is not well-defined), MRCKA (Myotonic dystrophy kinase-related CDC42 binding protein kinase alpha that may signal CDC42 control of the actin cytoskeleton and is related to DMPK), STK17A (Serine/threonine kinase 17A has apoptosis-inducing activity and is a member of the DAP kinase-related family), TLK2 (Tousled-like kinase 2 is involved in chromatin assembly and possibly DNA repair) and VRK2 (Vaccinia-related kinase 2 that is believed to regulate apoptosis and cell growth). Screening of the cBioPortal for Cancer Genomics (http://www.cbioportal.org/public-portal/) indicates amplification of MRCKA (CDC42BPA) in 13-25% of invasive breast cancer while TLK2 is amplified in 10% of invasive breast cancer and 25% of adenoid cystic breast cancer. ADCK1, DAPK3, DMPK STK17A and VRK2 were found to be similarly amplified in other cancers including prostate adenocarcinoma, uterine carcinosarcoma and pancreatic adenocarcinoma. Prominent MIB-binding signatures combined with potential increased expression in tumors suggests these understudied kinases have important functions for the tumor cell phenotype that have not been characterized to date.

The dynamic nature of the kinome is clearly captured in the kinase MIB-binding profiles characterizing baseline versus post-drug treated cells. This adaptive reprogramming of the kinome is involved in the epigenetic development of resistance to kinase inhibitors [22]. We have proposed that blocking this adaptive reprogramming is important clinically for making single kinase inhibitors more durable [6]. Pre- and post-drug treatment MIB/MS analysis allows for the quantitative measure of kinome adaptive responses and the rapid screening of combinations of kinase or epigenetic inhibitors that would block the adaptive behavior of the kinome [6], [9], [22]. This analysis can be done in preclinical models as well as patient trials where biopsy accessible tumor specimens are available. We have been able to capture more than 200 kinases with as little as 300 μg of tumor biopsy protein. Thus, MIBs provide a proteomic approach to characterize the functional state and dynamics of the kinome and thus define therapeutic response and targetable adaptive resistance networks. Importantly, MIBs capture both well-characterized and understudied kinases for a comprehensive measure of the functional kinome.

Materials and Methods

MIB affinity chromatography
Broad spectrum Type I kinase inhibitors (CTx-0294885, VI-16832, PP58, Purvalanol B, UNC-2147A, and UNC-8088A) were custom-synthesized with hydrocarbon linkers and terminal amine groups and covalently attached to ECH-activated Sepharose beads as previously described [6]. Cells were rinsed in PBS and processed in lysis buffer (50 mM HEPES, 150 mM NaCl, 0.5% Triton X-100, 1 mM EDTA, 1 mM EGTA, at pH 7.5 containing 10 mM NaF, 2.5 mM NaVO4, cOmplete protease Inhibitor Cocktail (Roche), and 1% Phosphatase Inhibitor Cocktails 2 and 3 (Sigma)). Tumor biopsies obtained from UNC Tissue Procurement were manually homogenized with a chilled mortar and pestle in lysis buffer. For individual bead profiling (Figure 1), 2mg of total protein was gravity-flowed over 100uL of each bead. For Figure 2 (cell lines), 5mg of total protein lysate and for Figure 4 (human tumor biopsies), 1mg of total protein was gravity-flowed over a mixture of the six kinase inhibitor-linked beads (175uL total beads). Beads were washed with at least 30 volumes of high salt (1M NaCl) and low salt (150mM NaCl) lysis buffer, then 500uL of low salt lysis buffer containing 0.1% SDS. Bound proteins were eluted by boiling with 0.5% SDS and 1% β-mercaptoethanol in 100mM Tris-HCl, pH 6.8, 2X 15 minutes, treated with DTT (5mM, 25min at 60°C) and Iodoacetamide (20mM, 30min in the dark at RT), and spin-concentrated to 100µL (Millipore Amicon Ultra-4, 10K cutoff) before Methanol/Chloroform precipitation. Proteins were trypsinized overnight at 37°C and then dried down in a speed-vac. Peptides were cleaned with C-18 spin columns (Pierce).

Mass Spectrometry and Analysis
Peptides were resuspended in 2% ACN and 0.1% Formic Acid. For Figure 1 (bead profiling) 20% of each sample was injected onto a Thermo Easy-Spray 75µm x 15cm C-18 column using an Easy nLC-1000 in technical triplicate and separated on a 150 min gradient (5-40% ACN). For Figures 2 and 4 (cell lines and tumor biopsies), 40% of the final peptide suspension was injected onto an Easy-Spray 75µm x 25cm C-18 column and separated on a 300min gradient (cell lines) or a 180min gradient (tumor biopsies). For all runs, ESI parameters: 3e6 AGC MS1, 80ms MS1 max inject time, 1e5 AGC MS2, 100ms MS2 max inject time, 20 loop count, 1.8 m/z isolation window, 45s dynamic exclusion. Spectra were searched against the Uniprot/Swiss-Prot database with Sequest HT on Proteome Discoverer software (Figures 1 and 2) or MaxQuant (Figure 4). Only peptides with medium or greater confidence (5% FDR) were considered for quantitation, and only kinases having 3 or more unique peptides were considered for further analysis. Heat maps were generated using GENE-E software (BROAD institute). Kinome trees were generated using Kinome Render (http://bcb.med.usherbrooke.ca/kinomerender.php).

RNA-seq
Total RNA was spin column purified using RNeasy Plus Mini kit (Qiagen). Library construction was performed at the UNC Lineberger Comprehensive Cancer Center Genomics Core and the sequencing at the UNC High-Throughput Sequencing Facility. mRNA-Seq libraries were constructed with 1 µg total RNA using the Illumina TruSeq™RNA Sample Prep Kit according to the manufacturer's protocol. 50-cycled single-end sequencing runs with multiplexing were produced using an Illumina HiSeq2000. CASAVA 1.8.2 generated bases and assessed sequence quality. The QC-passed reads were aligned to the hg19 human reference genome using MapSplice and the alignment profile was determined by Picard Tools v1.64 [23]. Aligned reads

were sorted and indexed using SAMtools, and then translated to transcriptome coordinates and filtered for indels, large inserts, and zero mapping quality using UBU v1.0. Transcript abundance estimates for each sample were determined using an Expectation-Maximization algorithm [24]. Publicly available data from [25], [26] were also processed using this computational method. Data is available in Data file S2.

Data analysis

Hierarchical clustering, Principal Components Analysis (PCA), and feature selection were performed in MATLAB. PCA is a commonly-used data analysis and dimension-reduction technique that transforms variables into a set of linearly uncorrelated principal components [27]. Application of PCA also provides the ability to assign a weight to each feature (kinase) in the data set that can be used as a relative measure of its ability to distinguish subtypes. To identify kinases that dominate individual PCs, kinases having weights in the 90th-percentile (i.e. those weighted in the top 10% of weights) per PC were selected from the first three PCs and used in downstream classification tasks. Feature selection using the Bhattacharyya distance was also used as a secondary mechanism for ranking kinases in terms of their ability to distinguish subtypes [21]. Pairwise classification between subtypes (e.g. basal-like subtype from all others, claudin-low from all others, etc) was iteratively performed to identify the most informative features.

Kinases identified through feature ranking and PCA are combined to create a list of the most distinguishing kinases in MIB-binding across the breast cancer subtypes. Subtype-specific signature kinases are defined as the top 5% of the highest ranking kinases found using the Bhattacharyya feature ranking coefficient for each subtype are compiled for the overall list. Pan-subtype signature kinases are defined as the most heavily weighted kinases (top 10%) from the first three PCs are used. Subtype-specific signature kinases are compiled from each of the breast cancer subtypes then the global signature kinases are added (in order from most heavily weighted to less heavily weighted) starting with PC1 kinases then moving to PC2 then to PC3 until a maximum of 50 kinases is reached to make up the list of distinguishing kinases. A total of 50 kinases was chosen as classification accuracy of the breast cancer subtypes plateaued at this level (Figure S1).

Comparison of MIB-binding to transcript abundance

The Z-score is calculated by sample based on the average log2 value per kinase and using the standard deviation of all kinases for a given sample; the samples within a particular subtype are then averaged (Figure 3 A-D). The Pearson correlation calculated by subtype (Figure 3 A—D) is the correlation between the MIB-binding profile to the RNA transcript levels within a single subtype. The Pearson correlation of individual kinases (Figure 3F) is calculated for each kinase across the 15 cell lines (not distinguished by subtype) between MIB-binding and RNA transcript levels. The correlation calculated by subtype (Figure 3 A—D) is the correlation between MIB-binding and RNA transcript levels to see how the profiles of each data type correlate between MIB-binding and RNA. The correlation calculated for each kinase is a correlation across cell lines to determine how a kinase correlates across all cell lines analyzed here.

Prediction of subtypes
Classification of subtype based on a previously unobserved kinome signature was performed using a Support Vector Machine (SVM). The SVM is a commonly used machine learning technique used in supervised classification, and thus requires a training set on which to learn parameters that can then be applied towards prediction of previously unobserved data [28]. The SVM used here was trained on the 50 distinguishing kinases previously identified. Performance of the SVM was analyzed using leave-one-out cross validation, where training is performed on all samples except for one and a classification prediction being carried out for the left-out sample. Predictions are made in this way for every sample and final sensitivity, specificity, and precision are calculated on classification performance across all samples. Human tumors are classified into one of the major groups (TNBC or HER2+/Luminal) or as "other" using the SVM trained on the 50 distinguishing kinases identified from breast cancer cell line samples.

Network Analysis
Protein-protein interaction information was compiled from multiple public data sources for the 254 kinases analyzed in this data set and included, the Human Integrated Protein-Protein Interaction rEference (HIPPIE) (updated 9/1/2015; [29]), Human Protein Reference Database (HPRD Release 9; [30]), Interlogous Interaction Database (I2D version 2.9; [31], [32]), PhosphoSitePlus (phosphosite.org - downloaded 10/15/2015; [33]) and Reactome protein-protein interactions (downloaded 12/15/2015; [34]). The union of all interactions between the 254 kinases was used to form a single network that was then clustered into communities/subnetworks with the spectral method in Mathematica (ver 10.3).

Supplementary Materials

Fig. S1. Classification accuracy across subtypes in LOOCV.

Table S1. Kinases bound to individual beads.

Table S2. Understudied kinases list.

Table S3. Precision, specificity, and sensitivity for all four subtypes in SVM.

Table S4. Kinases bound uniquely within a subtype.

Table S5. Kinases within subnetworks.

Data file S1. Baseline MIB-binding data matrix.

Data file S2. Matrix of RSEM values across cell lines.

Data file S3. MIB-binding response data matrix.

References

[1] "Comprehensive molecular portraits of human breast tumours.," *Nature*, vol. 490, no. 7418, pp. 61–70, Oct. 2012.

[2] A. Prat, B. Adamo, C. Fan, V. Peg, M. Vidal, P. Galván, A. Vivancos, P. Nuciforo, H. G. Palmer, S. Dawood, J. Rodón, S. Ramony Cajal, J. M. Del Campo, E. Felip, J. Tabernero, and J. Cortés, "Genomic analyses across six cancer types identify basal-like breast cancer as a unique molecular entity.," *Sci. Rep.*, vol. 3, p. 3544, Jan. 2013.

[3] K. A. Hoadley, C. Yau, D. M. Wolf, A. D. Cherniack, D. Tamborero, S. Ng, M. D. M. Leiserson, B. Niu, M. D. McLellan, V. Uzunangelov, J. Zhang, C. Kandoth, R. Akbani, H. Shen, L. Omberg, A. Chu, A. A. Margolin, L. J. van't Veer, N. Lopez-Bigas, P. W. Laird, B. J. Raphael, L. Ding, A. G. Robertson, L. a. Byers, G. B. Mills, J. N. Weinstein, C. Van Waes, Z. Chen, E. a. Collisson, C. C. Benz, C. M. Perou, and J. M. Stuart, "Multiplatform Analysis of 12 Cancer Types Reveals Molecular Classification within and across Tissues of Origin," *Cell*, vol. 158, no. 4, pp. 929–944, 2013.

[4] O. Fedorov, S. Müller, and S. Knapp, "The (un)targeted cancer kinome," *Nat. Chem. Biol.*, vol. 6, no. 3, pp. 166–169, Mar. 2010.

[5] J. S. Duncan, M. C. Whittle, K. Nakamura, A. N. Abell, A. A. Midland, J. S. Zawistowski, N. L. Johnson, D. A. Granger, N. V. Jordan, D. B. Darr, J. Usary, P.-F. Kuan, D. M. Smalley, B. Major, X. He, K. A. Hoadley, B. Zhou, N. E. Sharpless, C. M. Perou, W. Y. Kim, S. M. Gomez, X. Chen, J. Jin, S. V. Frye, H. S. Earp, L. M. Graves, and G. L. Johnson, "Dynamic Reprogramming of the Kinome in Response to Targeted MEK Inhibition in Triple-Negative Breast Cancer," *Cell*, vol. 149, no. 2, pp. 307–321, 2012.

[6] T. J. Stuhlmiller, S. M. Miller, J. S. Zawistowski, K. Nakamura, A. S. Beltran, J. S. Duncan, S. P. Angus, K. A. L. Collins, D. A. Granger, R. A. Reuther, L. M. Graves, S. M. Gomez, P.-F. Kuan, J. S. Parker, X. Chen, N. Sciaky, L. A. Carey, H. S. Earp, J. Jin, G. L. Johnson, "Inhibition of Lapatinib-Induced Kinome Reprogramming in ERBB2-Positive Breast Cancer by Targeting BET Family Bromodomains.," *Cell Rep.*, vol. 11, no. 3, pp. 390–404, Apr. 2015.

[7] A. A. Midland, M. C. Whittle, J. S. Duncan, A. N. Abell, K. Nakamura, J. S. Zawistowski, L. A. Carey, H. S. Earp III, L. M. Graves, S. M. Gomez, and G. L. Johnson, "Defining the expressed breast cancer kinome," *Cell Res.*, vol. 22, no. 4, pp. 620–623, Apr. 2012.

[8] H. Daub, J. V. Olsen, M. Bairlein, F. Gnad, F. S. Oppermann, R. Körner, Z. Greff, G. Kéri, O. Stemmann, and M. Mann, "Kinase-Selective Enrichment Enables Quantitative Phosphoproteomics of the Kinome across the Cell Cycle," *Mol. Cell*, vol. 31, no. 3, pp. 438–448, Aug. 2008.

[9] J. S. Duncan, M. C. Whittle, K. Nakamura, A. N. Abell, A. A. Midland, J. S. Zawistowski, N. L. Johnson, D. A. Granger, N. V. Jordan, D. B. Darr, J. Usary, P.-F. Kuan, D. M. Smalley, B. Major, X. He, K. A. Hoadley, B. Zhou, N. E. Sharpless, C. M. Perou, W. Y. Kim, S. M. Gomez, X. Chen, J. Jin, S V Frye, H. S. Earp, L. M. Graves, and G. L. Johnson, "Dynamic reprogramming of the kinome in response to targeted MEK inhibition in triple-negative breast cancer.," *Cell*, vol. 149, no. 2, pp. 307–21, Apr. 2012.

[10] J. E. Delmore, G. C. Issa, M. E. Lemieux, P. B. Rahl, J. Shi, H. M. Jacobs, E. Kastritis, T. Gilpatrick, R. M. Paranal, J. Qi, M. Chesi, A. C. Schinzel, M. R. McKeown, T. P. Heffernan, C. R. Vakoc, P. L. Bergsagel, I. M. Ghobrial, P. G. Richardson, R. A. Young, W. C. Hahn, K. C. Anderson, A. L. Kung, J. E. Bradner, C. S. Mitsiades, "BET bromodomain inhibition as a therapeutic strategy to target c-Myc.," *Cell*, vol. 146, no. 6, pp. 904–17, Sep. 2011.

[11] R. Marcotte, K. R. Brown, F. Suarez, A. Sayad, K. Karamboulas, P. M. Krzyzanowski, F. Sircoulomb, M. Medrano, Y. Fedyshyn, J. L. Y. Koh, D. van Dyk, B. Fedyshyn, M. Luhova, G. C. Brito, F. J. Vizeacoumar, F. S. Vizeacoumar, A. Datti, D. Kasimer, A. Buzina, P. Mero, C. Misquitta, J. Normand, M. Haider, T. Ketela, J. L. Wrana, R. Rottapel, B. G. Neel, and J. Moffat, "Essential gene profiles in breast, pancreatic, and ovarian cancer cells.," *Cancer Discov.*, vol. 2, no. 2, pp. 172–89, Feb. 2012.

[12] N. V. Jordan, A. Prat, A. N. Abell, J. S. Zawistowski, N. Sciaky, O. A. Karginova, B. Zhou, B. T. Golitz, C. M. Perou, and G. L. Johnson, "SWI/SNF chromatin-remodeling factor Smarcd3/Baf60c controls epithelial-mesenchymal transition by inducing Wnt5a signaling.," *Mol. Cell. Biol.*, vol. 33, no. 15, pp. 3011–25, Aug. 2013.

[13] A. Prat, M. C. U. Cheang, M. Martín, J. S. Parker, E. Carrasco, R. Caballero, S. Tyldesley, K. Gelmon, P. S. Bernard, T. O. Nielsen, and C. M. Perou, "Prognostic significance of progesterone receptor-positive tumor cells within immunohistochemically defined luminal A breast cancer.," *J. Clin. Oncol.*, vol. 31, no. 2, pp. 203–9, Jan. 2013.

[14] I. Hedenfalk, D. Duggan, Y. Chen, M. Radmacher, M. Bittner, R. Simon, P. Meltzer, B. Gusterson, M. Esteller, O. P. Kallioniemi, B. Wilfond, A. Borg, J. Trent, M. Raffeld, Z. Yakhini, A. Ben-Dor, E. Dougherty, J. Kononen, L. Bubendorf, W. Fehrle, S. Pittaluga, S. Gruvberger, N. Loman, O. Johannsson, H. Olsson, and G. Sauter, "Gene-expression profiles in hereditary breast cancer.," *N. Engl. J. Med.*, vol. 344, no. 8, pp. 539–48, Feb. 2001.

[15] C. Sotiriou, S.-Y. Neo, L. M. McShane, E. L. Korn, P. M. Long, A. Jazaeri, P. Martiat, S. B. Fox, A. L. Harris, and E. T. Liu, "Breast cancer classification and prognosis based on gene expression profiles from a population-based study.," *Proc. Natl. Acad. Sci. U. S. A.*, vol. 100, no. 18, pp. 10393–8, Sep. 2003.

[16] B. Zhang, J. Wang, XiaojingWang, J. Zhu, Q. Liu, Z. Shi, M. C. Chambers, L. J. Zimmerman, K. F. Shaddox, S. Kim, S. R. Davies, S. Wang, PeiWang, C. R. Kinsinger, R. C. Rivers, H. Rodriguez, R. R. Townsend, M. J. C. Ellis, S. a Carr, D. L. Tabb, R. J. Coffey, R. J. C. Slebos, D. C. Liebler, and the N. C. I. Cptac, "Proteogenomic characterization of human colon and rectal cancer," *Nature*, pp. 1–21, 2014.

[17] A. Sendoel, J. G. Dunn, E. H. Rodriguez, S. Naik, N. C. Gomez, B. Hurwitz, J. Levorse, B. D. Dill, D. Schramek, H. Molina, J. S. Weissman, and E. Fuchs, "Translation from unconventional 5′ start sites drives tumour initiation," *Nature*, 2017.

[18] R. de Sousa Abreu, L. O. Penalva, E. M. Marcotte, and C. Vogel, "Global signatures of protein and mRNA expression levels," *Mol. Biosyst.*, vol. 5, no. 12, pp. 1512–26, Dec. 2009.

[19] M. W. Karaman, S. Herrgard, D. K. Treiber, P. Gallant, C. E. Atteridge, B. T. Campbell, K. W. Chan, P. Ciceri, M. I. Davis, P. T. Edeen, R. Faraoni, M. Floyd, J. P. Hunt, D. J.

Lockhart, Z. V Milanov, M. J. Morrison, G. Pallares, H. K. Patel, S. Pritchard, L. M. Wodicka, and P. P. Zarrinkar, "A quantitative analysis of kinase inhibitor selectivity.," *Nat. Biotechnol.*, vol. 26, no. 1, pp. 127–32, Jan. 2008.

[20] M. I. Davis, J. P. Hunt, S. Herrgard, P. Ciceri, L. M. Wodicka, G. Pallares, M. Hocker, D. K. Treiber, and P. P. Zarrinkar, "Comprehensive analysis of kinase inhibitor selectivity.," *Nat. Biotechnol.*, vol. 29, no. 11, pp. 1046–51, Nov. 2011.

[21] A. Bhattacharyya, "On a Measure of Divergence between Two Statistical Populations Defined by Their Probability Distributions," *Bull. Calcutta Math. Soc.*, vol. 35, pp. 99–109, 1943.

[22] J. S. Zawistowski, S. M. Bevill, D. R. Goulet, T. J. Stuhlmiller, A. S. Beltran, J. F. Olivares-Quintero, D. Singh, N. Sciaky, J. S. Parker, N. U. Rashid, X. Chen, J. S. Duncan, M. C. Whittle, S. P. Angus, S. H. Velarde, B. T. Golitz, X. He, C. Santos, D. B. Darr, K. Gallagher, L. M. Graves, C. M. Perou, L. A. Carey, H. S. Earp, and G. L. Johnson, "Enhancer Remodeling During Adaptive Bypass to MEK Inhibition Is Attenuated by Pharmacological Targeting of the P-TEFb Complex," *Cancer Discov.*, 2017.

[23] K. Wang, D. Singh, Z. Zeng, S. J. Coleman, Y. Huang, G. L. Savich, X. He, P. Mieczkowski, S. A. Grimm, C. M. Perou, J. N. MacLeod, D. Y. Chiang, J. F. Prins, and J. Liu, "MapSplice: accurate mapping of RNA-seq reads for splice junction discovery.," *Nucleic Acids Res.*, vol. 38, no. 18, p. e178, Oct. 2010.

[24] B. Li and C. N. Dewey, "RSEM: accurate transcript quantification from RNA-Seq data with or without a reference genome.," *BMC Bioinformatics*, vol. 12, p. 323, Jan. 2011.

[25] A. Daemen, O. L. Griffith, L. M. Heiser, N. J. Wang, O. M. Enache, Z. Sanborn, F. Pepin, S. Durinck, J. E. Korkola, M. Griffith, J. S. Hur, N. Huh, J. Chung, L. Cope, M. Fackler, C. Umbricht, S. Sukumar, P. Seth, V. P. Sukhatme, L. R. Jakkula, Y. Lu, G. B. Mills, R. J. Cho, E. A. Collisson, L. J. van't Veer, P. T. Spellman, and J. W. Gray, "Modeling precision treatment of breast cancer," *Genome Biol.*, vol. 14, no. 10, p. R110, 2013.

[26] L. M. Heiser, A. Sadanandam, W.-L. Kuo, S. C. Benz, T. C. Goldstein, S. Ng, W. J. Gibb, N. J. Wang, S. Ziyad, F. Tong, N. Bayani, Z. Hu, J. I. Billig, A. Dueregger, S. Lewis, L. Jakkula, J. E. Korkola, S. Durinck, F. Pepin, Y. Guan, E. Purdom, P. Neuvial, H. Bengtsson, K. W. Wood, P. G. Smith, L. T. Vassilev, B. T. Hennessy, J. Greshock, K. E. Bachman, M. A. Hardwicke, J. W. Park, L. J. Marton, D. M. Wolf, E. A. Collisson, R. M. Neve, G. B. Mills, T. P. Speed, H. S. Feiler, R. F. Wooster, D. Haussler, J. M. Stuart, J. W. Gray, and P. T. Spellman, "Subtype and pathway specific responses to anticancer compounds in breast cancer.," *Proc. Natl. Acad. Sci. U. S. A.*, vol. 109, no. 8, pp. 2724–9, Feb. 2012.

[27] M. D. Slack, E. D. Martinez, L. F. Wu, and S. J. Altschuler, "Characterizing heterogeneous cellular responses to perturbations.," *Proc. Natl. Acad. Sci. U. S. A.*, vol. 105, no. 49, pp. 19306–11, Dec. 2008.

[28] T. S. Furey, N. Cristianini, N. Duffy, D. W. Bednarski, M. Schummer, and D. Haussler, "Support vector machine classification and validation of cancer tissue samples using microarray expression data.," *Bioinformatics*, vol. 16, no. 10, pp. 906–14, Oct. 2000.

[29] M. H. Schaefer, J.-F. Fontaine, A. Vinayagam, P. Porras, E. E. Wanker, M. A. Andrade-

Navarro, "HIPPIE: Integrating Protein Interaction Networks with Experiment Based Quality Scores," *PLoS One*, vol. 7, no. 2, p. e31826, Feb. 2012.

[30] T. S. Keshava Prasad, R. Goel, K. Kandasamy, S. Keerthikumar, S. Kumar, S. Mathivanan, D. Telikicherla, R. Raju, B. Shafreen, A. Venugopal, L. Balakrishnan, A. Marimuthu, S. Banerjee, D. S. Somanathan, A. Sebastian, S. Rani, S. Ray, C. J. Harrys Kishore, S. Kanth, M. Ahmed, M. K. Kashyap, R. Mohmood, Y. L. Ramachandra, V. Krishna, B. A. Rahiman, S. Mohan, P. Ranganathan, S. Ramabadran, R. Chaerkady, and A. Pandey, "Human Protein Reference Database--2009 update.," *Nucleic Acids Res.*, vol. 37, no. Database issue, pp. D767–72, Jan. 2009.

[31] K. R. Brown and I. Jurisica, "Online Predicted Human Interaction Database," *Bioinformatics*, vol. 21, no. 9, pp. 2076–2082, May 2005.

[32] K. R. Brown and I. Jurisica, "Unequal evolutionary conservation of human protein interactions in interologous networks," *Genome Biol.*, vol. 8, no. 5, p. R95, 2007.

[33] P. V Hornbeck, B. Zhang, B. Murray, J. M. Kornhauser, V. Latham, and E. Skrzypek, "PhosphoSitePlus, 2014: mutations, PTMs and recalibrations.," *Nucleic Acids Res.*, vol. 43, no. Database issue, pp. D512–20, Jan. 2015.

[34] D. Croft, A. F. Mundo, R. Haw, M. Milacic, J. Weiser, G. Wu, M. Caudy, P. Garapati, M. Gillespie, M. R. Kamdar, B. Jassal, S. Jupe, L. Matthews, B. May, S. Palatnik, K. Rothfels, V. Shamovsky, H. Song, M. Williams, E. Birney, H. Hermjakob, L. Stein, and P. D'Eustachio, "The Reactome pathway knowledgebase.," *Nucleic Acids Res.*, vol. 42, no. Database issue, pp. D472–7, Jan. 2014.

Acknowledgments

Funding: MH104999 (GLJ, SMG), CA058223 (GLJ), GM101141 (GLJ, LMG), Susan G. Komen Foundation IIR2-225201 (GLJ), GM116534 (SMB), Komen Foundation PDF15331014 (SHV), UNC Junior Faculty Development Award (JSZ), University Research Council Small Grant Award (JSZ), University Cancer Research Fund (GLJ). **Author contributions**: KALC did computational analysis, generated figures, writing, and editing. TS generated experimental (MIB/MS) data, created figures, writing, and editing. JSZ generated experimental (RNA-seq), writing, and editing. MPE did writing and editing. TP generated experimental (MIB/MS) data. CRH generated growth curves, writing, and editing. DRG generated experimental (MIB/MS) data, writing, and editing. SMB generated experimental (MIB/MS) data, writing, and editing. SPA generated experimental (MIB/MS) data, writing, and editing. SHV generated experimental (MIB/MS) data, writing, and editing. NS analyzed RNA-seq data in pipeline, writing, and editing. LMG involved in experimental design. GLJ managed and designed experimental work, writing, and editing. SMG managed computational analyses, writing, and editing. **Competing interests**: The authors do not have any competing interests. **Data and materials availability**: All processed data is provided in Supplementary Data Files. Data from the Sequence Read Archive is used for some analyses here: SRX317702, SRX317711, SRX317712, SRX317715, SRX317717, SRX317723, SRX317730, SRX317733, SRX317736, SRX317738PT1, SRX317738PT2, SRX317741, SRX317743, SRX317747.

Figures and Tables

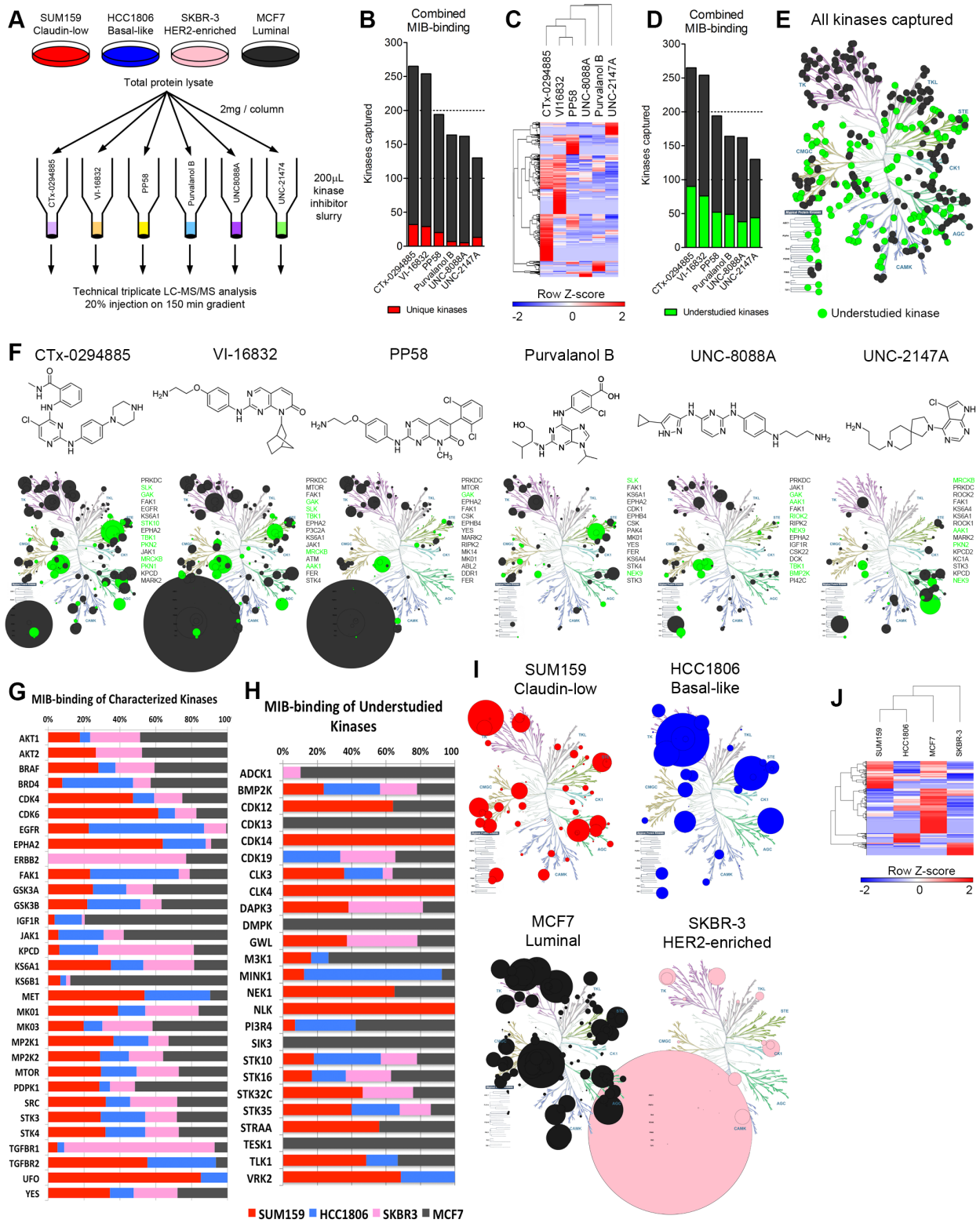

Fig. 1. Assessment of multiplexed kinase inhibitor beads (MIBs) for kinase capture across breast cancer subtypes. (A) Experimental design to assess performance of six kinase inhibitor

beads. (B) Combined data from all four cell lines assayed shows CTx-0294885 binds the most number of kinases. Number of kinases captured uniquely by each bead is shown in red. (C) Euclidean hierarchical clustering kinase peptides bound by the six beads shows each bead enriches for a distinct set of kinases. UNC-2147A displays the most unique binding profile. (D) A large proportion of kinases captured by MIBs (23-24%) are understudied or poorly characterized (green). (E) 381 kinases were identified across all four cell lines, including 346 protein kinases and 35 metabolic kinases. Of these protein kinases, 142 are understudied (green). (F) Chemical structures and kinase-binding of each inhibitor bead across the kinome. Circle size is proportional to the number of unique peptides identified per kinase. PRKDC (DNA-PK) is over-represented in VI-16832 and PP58 (large circle under Atypical protein kinases). Most beads capture kinases across families but UNC-2147 preferentially enriches for AGC family kinases. Shown to the right of each kinome tree are the 15 most-highly captured kinases for each bead. Green circles and text signifiy understudied kinases. (G) Comparison of relative binding of characterized kinases across breast cancer cell lines/subtypes. (H) Comparison of relative binding of understudied kinases across breast cancer cell lines/subtypes. (I) Each cell line representing the different breast cancer subtypes displays a unique kinome profile. Only kinases with the greatest number of peptides identified in particular cell line are shown. Cirlce size is proportional to the number of peptides identified. (J) Hierarchical clustering of peptides identified for each kinase (rows) across the cell lines (columns) cluster triple-negative cell lines (SUM159, HCC1806) together and indicates HER2-positive SKBR3 cells have the most distinct kinome profile.

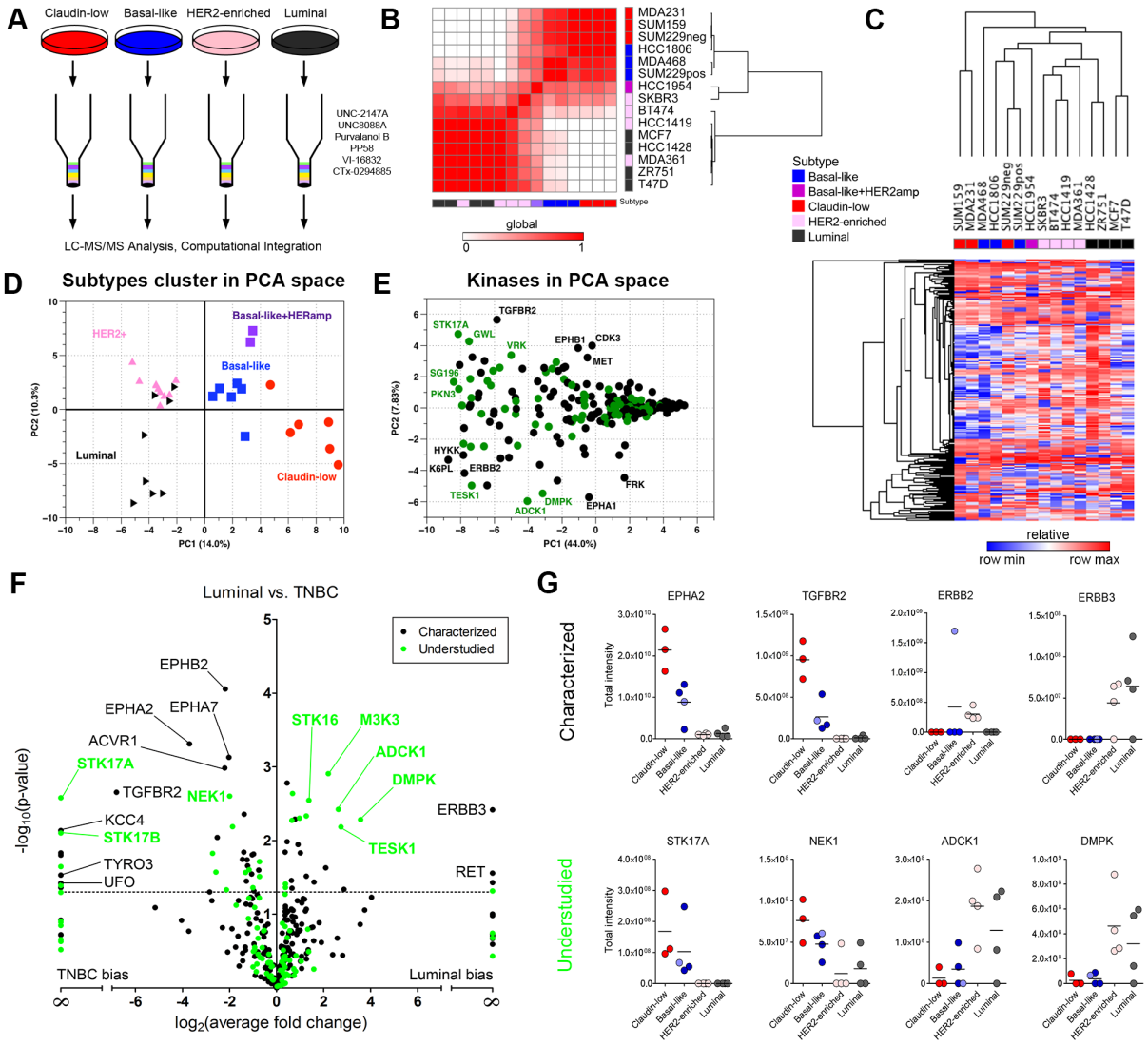

Fig. 2. MIB/MS kinome profiling assigns breast cancer cell lines to functional subtypes. (A) Individual samples run across 6-bead composition with LC-MS/MS analysis. (B) Heat map of correlation between MIB/MS samples for cell lines analyzed. Color bars indicated the subtype of each cell line (blue: basal-like, red: claudin-low, pink: HER2-enriched, black: luminal, purple: basal-like/HER2amp). White in the heat map indicates a low correlation between samples, while red shows higher correlation. Rows and columns are hierarchically clustered. (C) Heat map of MIB/MS average for each of the 15 cell lines analyzed. Rows are kinases; columns are MIB/MS cell line averages. Color bar for columns indicates the subtype associated to each cell line. Each column is an average of 2 or 3 MIB/MS samples, depending on the cell line. Colors in the heat map are relative by row minimum (blue) and maximum (red). A total of 254 kinases passed filtering (see Methods). Rows and columns are hierarchically clustered using Euclidean distance and average linkage. (D) Principal Component Analysis (PCA) on the entire MIB/MS data set. PC1 and PC2 account for 14.0% and 10.3% of the variance in the data set, respectively. A total of 32 samples across the fours subtypes are represented by their subtype (red circle: claudin-low, blue square: basal-like, pink upward triangle: HER2-

enriched, black right-pointing triangle: luminal, purple square: basal-like/HER2amp). (E) PCA on the MIB/MS data set to show highly variable kinases across the samples. Characterized and understudied kinases are shown in black and green, respectively. PC1 and PC2 account for 44.0% and 7.83% of the variance in the data set, respectively. (F) Volcano plot showing characterized (black) and understudied (green) kinases that are significantly ($p<0.05$) different between the Luminal/HER2-enriched and TNBC (basal-like/claudin-low) cell line samples in the MIB/MS data set. (G) Profiles of selected characterized (top row) and understudied (bottom row) kinases across breast cancer subtypes.

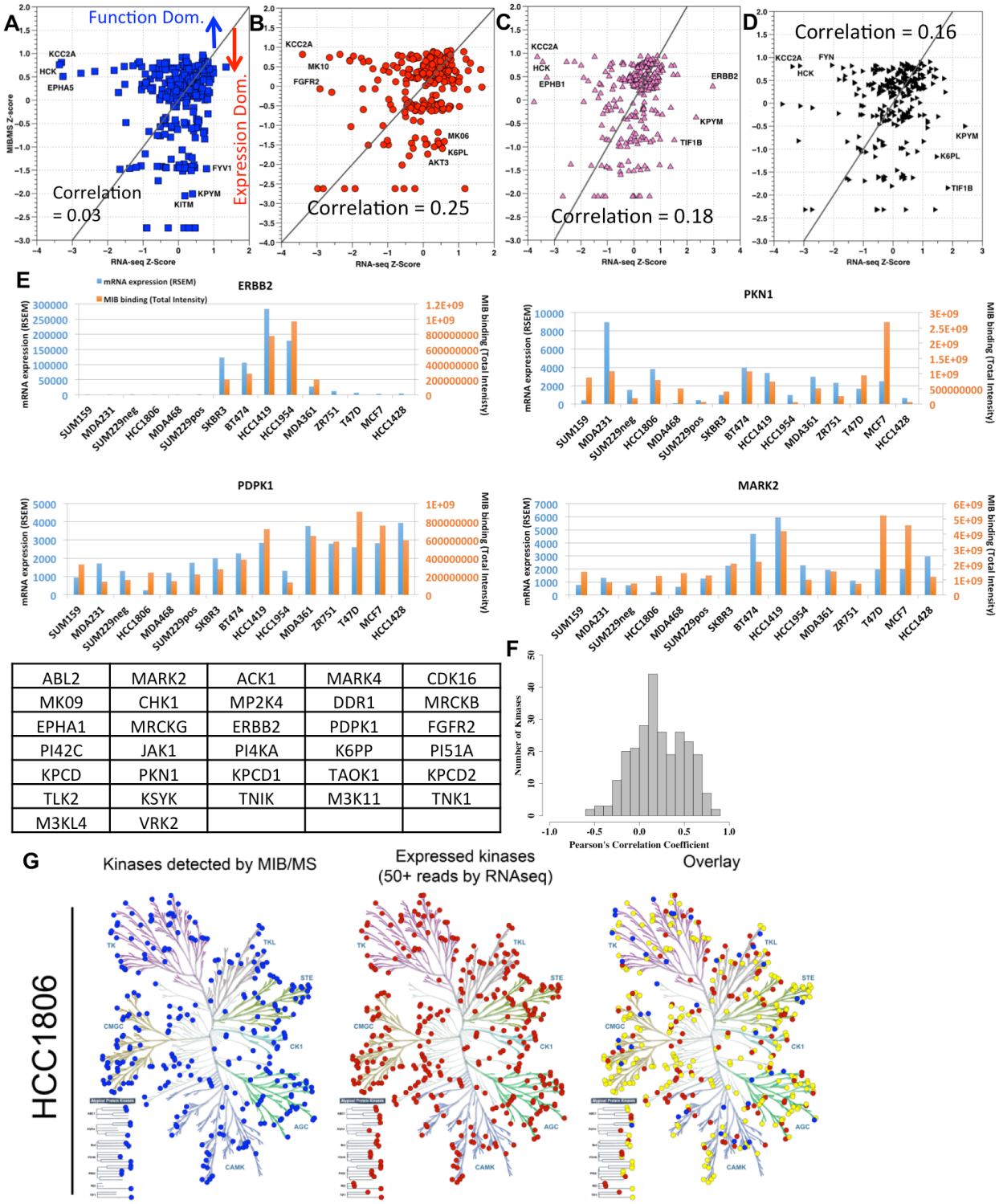

ABL2	MARK2	ACK1	MARK4	CDK16
MK09	CHK1	MP2K4	DDR1	MRCKB
EPHA1	MRCKG	ERBB2	PDPK1	FGFR2
PI42C	JAK1	PI4KA	K6PP	PI51A
KPCD	PKN1	KPCD1	TAOK1	KPCD2
TLK2	KSYK	TNIK	M3K11	TNK1
M3KL4	VRK2			

Fig. 3. Overall MIB-binding and mRNA expression levels are not correlated. (A—D) Comparison of baseline normalized MIB/MS (y-axis) intensities and baseline normalized mRNA (x-axis) counts in cell lines for representing each of the four subtypes (A: basal-like, B: claudin-low, C: HER2-enriched, D: luminal). The grey line indicates a 1-to-1 relationship between normalized MIB/MS and RNA levels. Above the line indicates

Function Dominance, while below the line indicates Expression Dominance. Correlation between the MIB/MS and RNA levels were basal-like: 0.03, claudin-low: 0.25, HER2-enriched: 0.18, and luminal: 0.16. (E) Representative raw profiles of ERBB2, PKN1, PDPK1, and MARK2 in MIB/MS intensity (orange bars) and mRNA RSEM counts (bue bars), which are both highly correlated between the two data sets (correlation > 0.8). A table of 32 kinases that have a correlation greater than 0.7 across the four subtypes is also shown (bottom). (F) Frequency distribution of Pearson's correlation coefficient across all cell lines in MIB/MS and RNA-seq for each of the 254 kinases. (G) KinomeTrees for MIB-binding (left), RNA expression (middle), and the overlap between the two data sets (right) for the HCC1806 (basal-like) cell line. In the overlap, yellow indicates where the two data sets overlap.

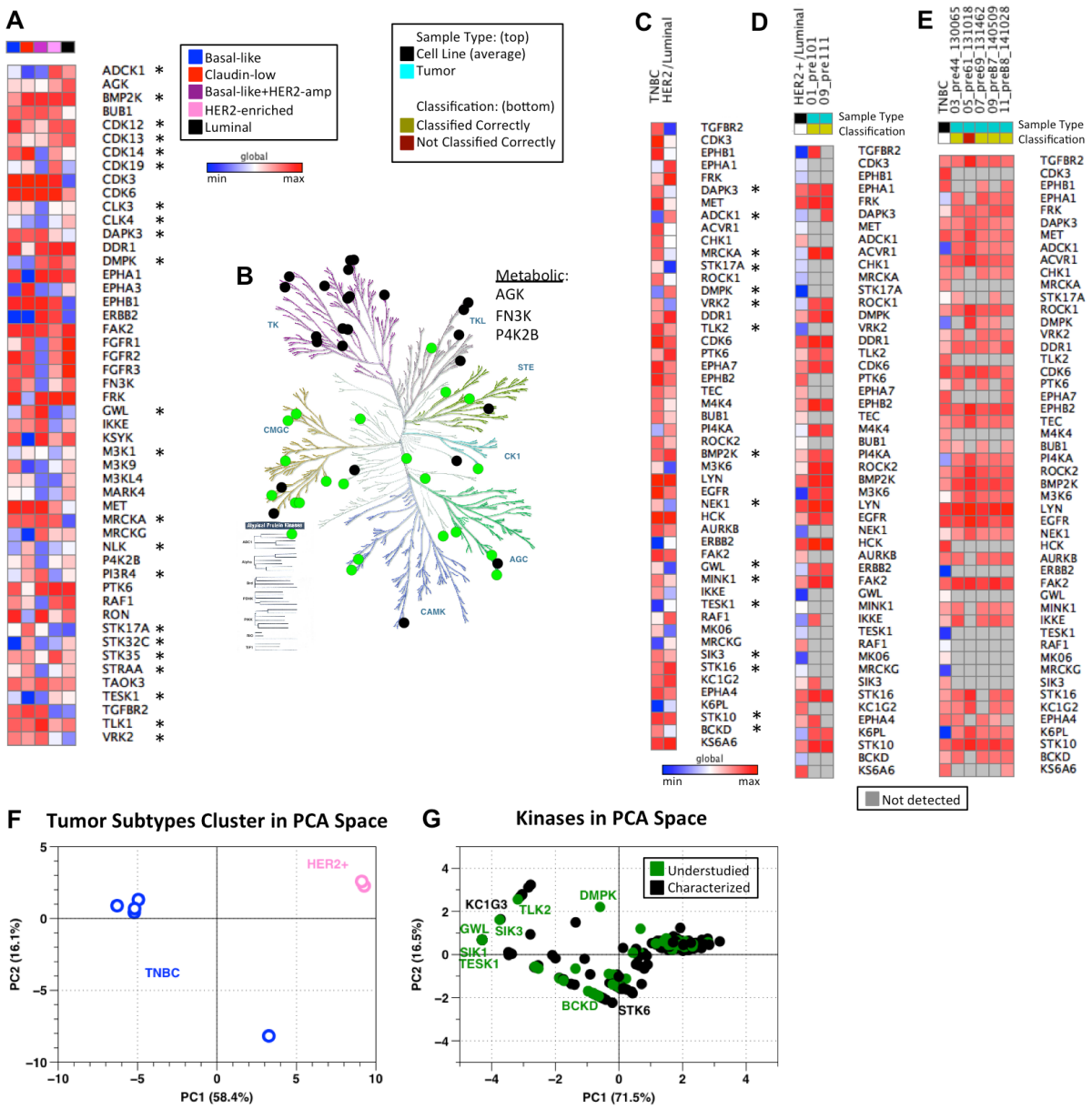

Fig. 4. Baseline kinome of cell lines and tumors across breast cancer subtypes. (A) Compilation of subtype specific and pan-subtype kinases chosen from feature selection and PCA, respectively. All data is log2 normalized and autoscaled by sample, with heat map colors indicating low (blue) to high (red) MIB-binding. Column color bar indicates subtype (red: claudin-low, blue: basal-like, pink: HER2-enriched, black: luminal, purple: basal-like/HER2amp; Understudied kinases are denoted by *). Global maximum and minimum color assignment. (B) KinomeTree with the 50 distinguishing features from (A) are denoted. Black circles denote characterized kinases, while green circles represent understudied kinases. (C) Kinases chosen from feature selection when comparing Luminal/HER2-enriched cell line samples against basal-like/claudin-low (TNBC) cell line samples. Kinases are ordered from top to bottom in the same ordering as from the feature selection (most heavily weighted kinases are at the top of the heat map). All data

is log2 normalized and autoscaled by sample, with heat map colors consisten with those in (A) (Understudied kinases are denoted by *). Global maximum and minimum color assignment. (D) Heat map of Luminal/HER2-enriched cell line average (HER2+/Luminal column; black in "Sample Type" column color bar) across the kinases shown in (C) with two tumor samples (teal in "Sample Type" column color bar). Data is log2 normalized and autoscaled by samples, as previously noted. Yellow in the "Classification" column bar shows which samples are classified correctly as Luminal/HER2-enriched by the SVM using the kinases from (C). Blue in the heat map indicates a low MIB-binding, red indicates high MIB-binding, and grey (in the tumor samples only) indicates that a kinase was not detected by MIBs in the tumor sample. Global maximum and minimum color assignment. (E) Heat map of TNBC cell line average (TNBC column; black in "Sample Type" column color bar) across the kinases shown in (C) with five tumor samples (teal in "Sample Type" column color bar). Data is log2 normalized and autoscaled by samples, as previously noted. Yellow in the "Classification" column color bar shows which samples are classified correctly as TNBC by the SVM using the kinases from (C). Dark red in "Classification" indicates that the tumor sample was incorrectly classified (not classified as TNBC) by the SVM using the kinases identified in (C). Color scheme in the heatmap is consistent with that described in (D). Global maximum and minimum color assignment. (F) PCA scores plot of tumor samples with PC1 and PC2 accounting for 58.4% and 16.1% of variance, respectively. TNBC tumors are blue and HER2-enriched tumors are pink. (G) PCA loadings plot of tumor samples with PC1 and PC2 accounting for 71.5% and 16.5% of variance, respectively. Black points are characterized kinases and green points denote understudied kinases.

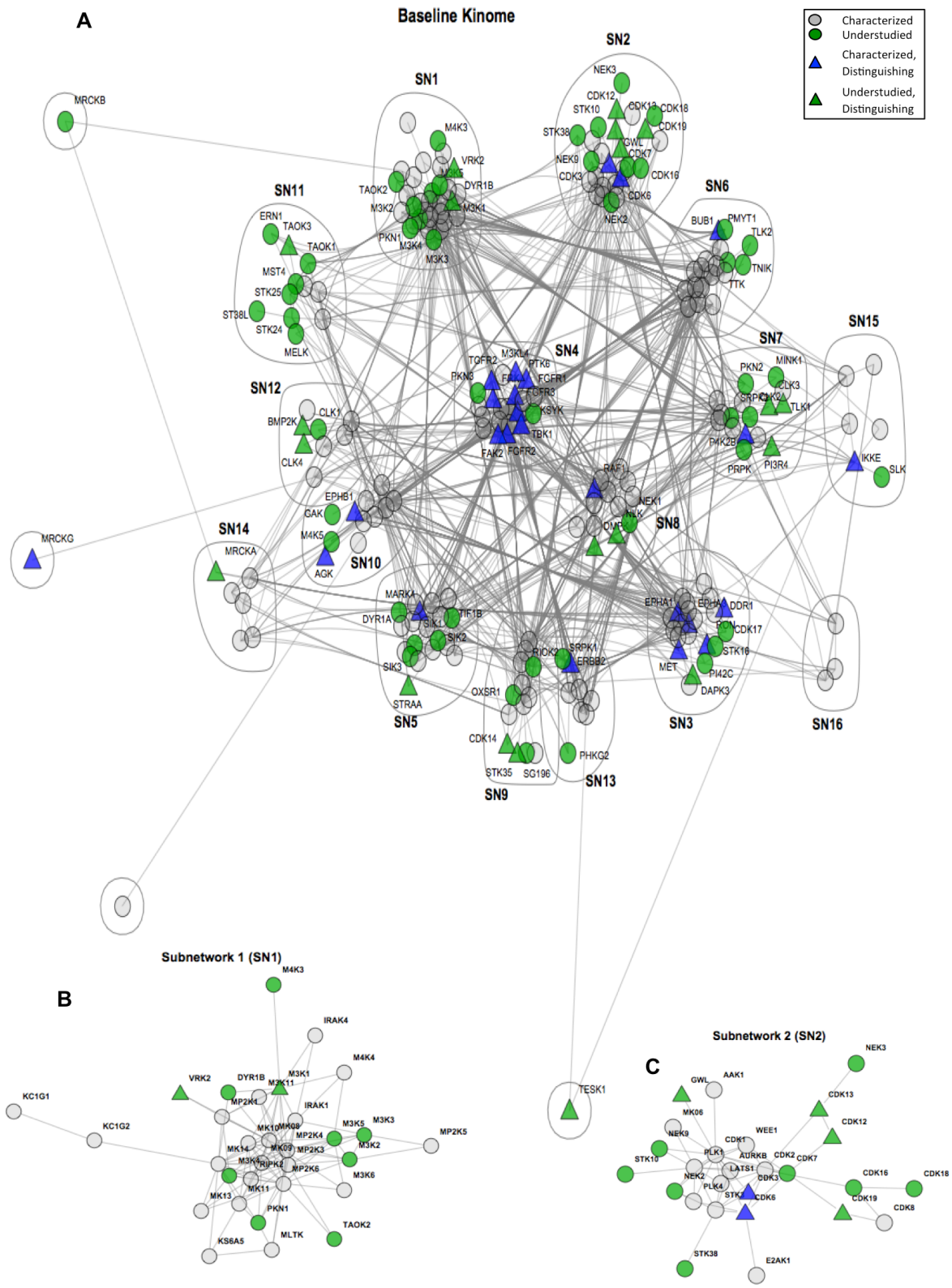

Fig. 5. Subnetworks in the functional kinome. (A) Compiled and clustered protein-protein interaction network from public data sources of the 254 kinases analyzed in the MIB/MS cell line data set. Green nodes represent understudied kinases, while grey and blue nodes

represent characterized kinases. Triangles are kinases that are also in the distinguishing features found in Figure 4A. (B) The largest subnetwork in (A) that contains understudied (10 kinases; 34.5%) and distinguishing (2 kinases; 6.9%) kinases. This subnetwork is enriched for the GO term “Innate Immune Response”. (C) The second largest subnetwork within (A) that contains 12 (41.4%) understudied and 6 (20.7%) distinguishing kinases and is enriched for “Cell Cycle”, “Cell Division”, and “Mitosis” GO terms.

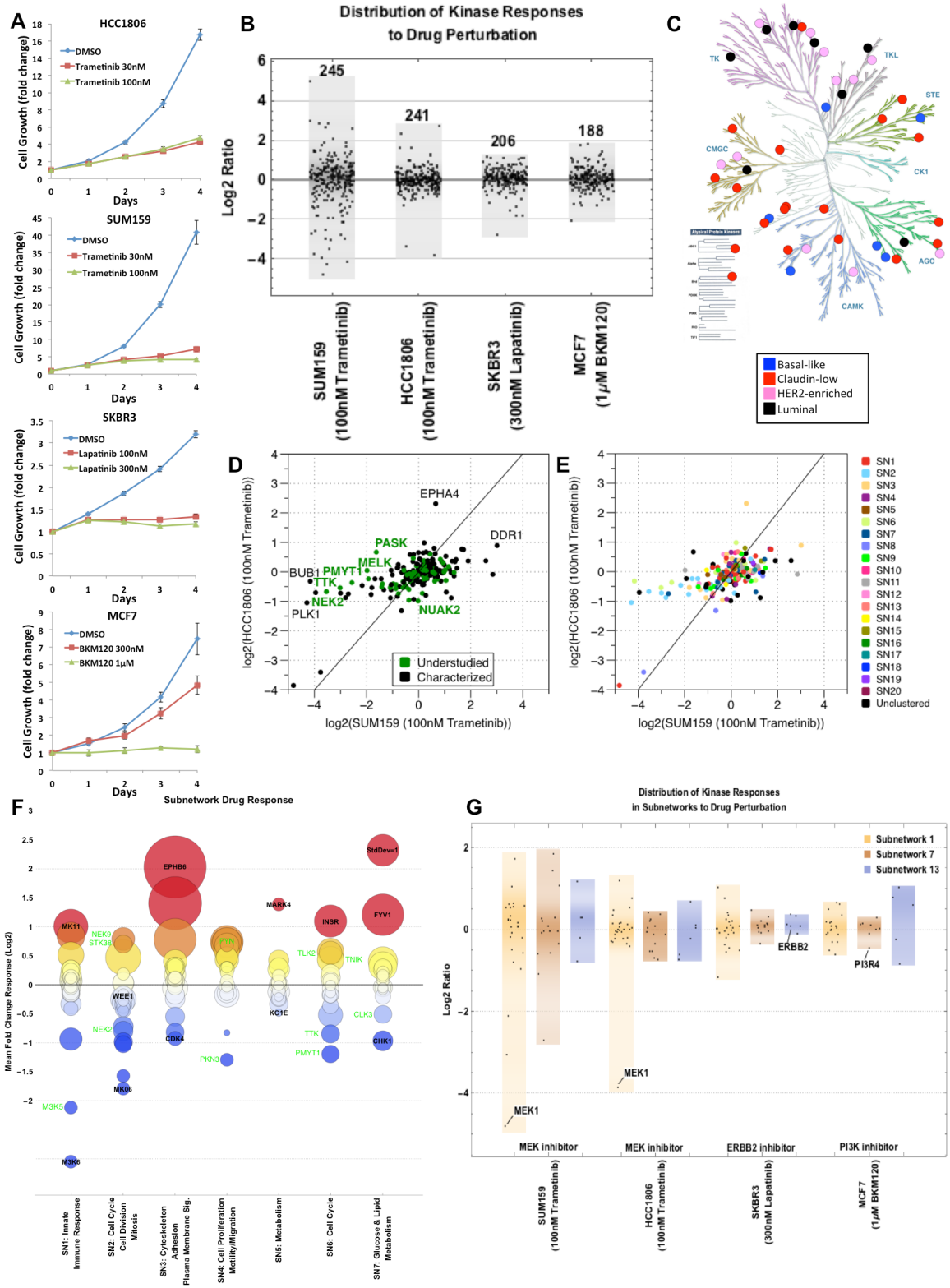

Fig. 6. Kinome drug response overall and by subnetwork. (A) Growth curves for HCC1806 + Trametinib, SUM159 + Trametinib, SKBR3 + Lapatinib, and MCF7 + BKM120. All curves were done at two different doses. (B) Repsonse of kinome in representative cell

lines across four subtypes of breast cancer (claudin-low: SUM159, basal-like: HCC1806, HER2-enriched: SKBR3, luminal: MCF7) when treated with the indicated kinase inhibitor. Distribution of the kinome response on the log2-scale is shown for each cell line/subtype; each point represents a kinase. (C) KinomeTree showing the kinases that are uniquely captured in each of the subtypes in the baseline data set. Blue circles denote kinases bound to the MIBs only in basal-like samples. Similarly, red circles represent claudin-low, pink circles represent HER2-enriched, and black circles represent luminal uniquely bound kinases. (D) Scatter plot of the response of the basal-like vs. claudin-low cell lines to treatment with 100nM Trametinib. All values are fold change to untreated cells and log2-transformed. Kinase points are colored black for characterized and green for understudied. (E) Scatter plot of the response of the basal-like vs. claudin-low cell lines to treatment with 100nM Trametinib (same as in (D)). Kinases are colored by subnetwork assigned to each kinase from Figure 5. (F) Subnetwork response to drug perturbation showing mean fold change across the four representative cell lines (SUM159, HCC1806, SKBR3, and MCF7) for the top 7 subnetworks identified from Figure 5. Characterized and understudied kinases in each subnetwork are labeled in black and green, respectively. The color of each circle indicates the mean fold change (red=high/above 0, blue=low/below 0), while the area of the circle denotes the standard deviation of the fold changes across the representative cell lines. (G) Distribution of the kinome response in the three subnetworks (SN1, SN7, and SN13 on the log2-scale is show for each cell line/subtype.